J Mol Model (2011) 17:785–794
DOI 10.1007/s00894-010-0769-6

ORIGINAL PAPER

Predicting helium and neon adsorption and separation on carbon nanotubes by Monte Carlo simulation

Zabiollah Bolboli Nojini · Amir Abbas Rafati · Seyed Majid Hashemianzadeh · Sepideh Samiee

Received: 4 March 2010 / Accepted: 25 May 2010 / Published online: 18 June 2010

Abstract The adsorption of helium and neon mixtures on single-walled carbon nanotubes (SWCNTs) was investigated at various temperatures (subcritical and supercritical) and pressures using canonical Monte Carlo (CMC) simulation. Adsorption isotherms were obtained at different temperatures (4, 40, 77 and 130 K) and pressures ranging from 1 to 16 MPa. Separation factors and isosteric enthalpies of adsorption were also calculated. Moreover, the adsorption isotherms were obtained at constant specific temperatures (4 and 40 K) and pressures (0.2 and 1.0 MPa) as a function of the amount adsorbed. All of the adsorption isotherms for an equimolar mixture of helium and neon have a Langmuir shape, indicating that no capillary condensation occurs. Both the helium and the neon adsorption isotherms exhibit similar behavior, and slightly more of the helium and neon mixture is adsorbed on the inner surfaces of the SWCNTs than on their outer surfaces. More neon is adsorbed than helium within the specified pressure range. The data obtained show that the isosteric enthalpies for the adsorption of neon are higher than those for helium under the same conditions, which means that adsorption of neon preferentially occurs by (15, 15) SWCNTs. Furthermore, the isosteric enthalpies of adsorption of both gases decrease with increasing temperature.

Keywords Adsorption · Molecular simulation · Carbon nanotube · Separation factor · Isosteric enthalpy of adsorption

Z. Bolboli Nojini (✉)
Department of Chemistry, Faculty of Science,
Shahid Chamran University,
Ahvaz, Iran
e-mail: zb.nojini@gmail.com
e-mail: zb_nojini@scu.ac.ir

A. Abbas Rafati · S. Samiee
Faculty of Chemistry, Bu-Ali Sina University,
Hamedan, Iran

S. Majid Hashemianzadeh
Molecular Simulation Research Laboratory, Department of Chemistry, Iran University of Science and Technology,
Tehran, Iran

Introduction

Gas adsorption on carbon nanotubes has been the subject of intense attention from researchers in recent years [1]. Several experimental and theoretical studies have been performed with the aim of understanding how adsorbed gases behave on these novel materials. Although many detailed studies related to the adsorption of small and spherical molecules on nanotubes have been performed [2–11], reports on the adsorption of hydrocarbons (with the exception of methane), especially linear molecules, have been rather limited [12–16]. Interest in these systems also stems from their widespread use in the petrochemical industry. In the past two decades, the problem of clean energy storage on light nanoporous materials has received considerable attention due to the well-known "greenhouse effect" caused by the increase in the concentrations of atmospheric gas pollutants (CO_2, SO_2, CH_4, CFCs, etc.). The potential for carbon nanotubes (CNTs) [17, 18] and other nanomaterials to be used as a means of fuel gas (mainly H_2) storage has been understood since the earliest days of nanotube research, and numerous efforts directed at this aim have been conducted through experimental [19–24] and theoretical [25, 26] techniques, including computer simulations [27–32]. The adsorption of gases

onto the inner surfaces of microporous materials forms the basis for many industrial processes of gas purification and separation [29–32]. The purification of rare gases is also of great industrial interest, since there are both medical and lighting applications of xenon. Mueller et al. [33] measured the volume-specific uptake of rare gases by IRMOF-1, and showed that this MOF exhibits preferential adsorption of xenon over lighter rare gases. In addition, they found that Cu-BTC, also known as HKUST-1, can be used to separate xenon from krypton, with a calculated capacity of more than 60 wt%, thus exceeding the levels achieved by high-surface-area carbons. Mixtures of rare gases absorb in the microwave and far-infrared regions of the spectrum due to the dipoles induced in dissimilar pairs, for example individual Ar and Ne atoms, during collisional interactions [34]. This phenomenon has also been studied in small atomic clusters [35, 36] using computer simulation methods. Many theoretical and experimental attempts have focused on the adsorption of rare gases on microporous materials [37–42].

In our previous works [43, 44], we studied the adsorption of gases (O_2, N_2, and NO) on the outer and inner surfaces of SWCNTs using DFT calculations. In those studies, we employed quantum mechanics to investigate gas adsorption on nanotubes. In addition, we studied the adsorption of O_2 and N_2 mixtures on nanotubes using Monte Carlo simulation [45].

In the thermodynamic state (T and P), the thermal wavelength of helium and neon is given by $\Lambda=h/(2\pi mkT)^{0.5}$ (h is the Planck constant, m is the mass of the helium and neon, and k is the Boltzmann constant). The value of Λ is such that quantum effects can modify estimates of thermodynamic properties such as adsorption obtained by classical simulation. The main purpose of this work was to obtain an estimate of the helium and neon adsorption and separation on (15, 15) SWCNTs using classical canonical Monte Carlo (MC) simulation.

Simulation procedure

The intermolecular interaction was modeled by the isotropic pairwise additive site-site Lennard–Jones (LJ) potential:

$$\varphi_{LJ}(r) = 4\varepsilon_{ff}\left[\left(\frac{\sigma_{ff}}{r}\right)^{12} - \left(\frac{\sigma_{ff}}{r}\right)^{6}\right], \quad (1)$$

where ε_{ff} and σ_{ff} are the energy and length parameters in the LJ potential, and r denotes the center-to-center distance. The subscript ff denotes interactions between two fluid molecules, and ϕ_{LJ} represents the full LJ potential. The total potential for interactions between gas molecules and SWCNTs was calculated using the site–site interaction method [45]:

$$\varphi_{fw} = 4\varepsilon_{fw}\sum_{i==1}^{N_f}\sum_{j=1}^{N_{carbon}}\left[\left(\frac{\sigma_{fw}}{r_{ij}}\right)^{12} - \left(\frac{\sigma_{fw}}{r_{ij}}\right)^{6}\right], \quad (2)$$

where N_f is the total number of gas molecules, N_{carbon} is the total number of carbon atoms at the wall, and r_{ij} is the center-to-center distance between the gas and the carbon atoms in the SWCNTs. The subscript fw denotes interactions between a fluid molecule and a carbon wall. Cross parameters of the unlike pair of particles i and j were obtained using the Lorentz–Berthelot mixing rules:

$$\varepsilon_{ij} = \sqrt{\varepsilon_i\varepsilon_j} \quad \sigma_{ij} = (\sigma_i + \sigma_j)/2. \quad (3)$$

Similarly, the LJ potential parameters used to model nanotube–He and nanotube–Ne interactions were obtained using Eq. 3. All of the interatomic potential parameters are given in Table 1. CMC simulations with a fixed number of gas molecules N, a volume V and a temperature T were carried out to investigate the adsorption of He and Ne mixtures on the (15, 15) SWCNTs. Further details of the method used can be found elsewhere [48, 49].

In this work, a metallic armchair-type SWCNT with a highly symmetrical structure, i.e., (15, 15) with 1230 atoms and diameter of 20.197 Å, was selected. The C–C bonds were assumed to be rigid and fixed at 1.41 Å in length. The noble gas molecules were taken to be spherically symmetric and uncharged Lennard–Jones particles, and intermolecular interactions were modeled only with Van der Waals potential parameters. We considered gas adsorption at subcritical and supercritical temperatures (4, 40, 77, and 130 K) for the pressure range 0.5–16 MPa.

Adsorption is usually analyzed as a function of bulk pressure, so an accurate equation of state (EOS) or simulations of the bulk phase are needed to convert chemical potential to bulk pressure. However, an accurate EOS may not be available, and additional simulations are not straightforward and may be time-consuming, especially for the wide range of temperatures, pressures, and compositions needed for mixtures. For this reason, the ideal gas assumption of the bulk phase is usually used; however, this assumption may not be accurate.

Table 1 LJ potential parameters [46 and 47]

Species	ε/k_B (K)	σ (Å)
He–He	10.20	2.56
Ne–Ne	36.83	2.79
C–C	28.20	3.40
C–He	16.96	2.98
C–Ne	32.23	3.10
He–Ne	19.38	2.67

The common feature shared by all Monte Carlo simulations is that a Markov chain of molecular configurations is produced. Any properties of interest can be obtained by averaging over this chain. A Monte Carlo move consists of either the translation of a molecule or the rotation of a molecule. Two different moves were used to generate the Markov chain, which is composed of a series of molecular configurations [48, 49]. The first move is the displacement of a molecule; a molecule was selected at random and a random displacement was assigned. The second move is the rotation of a molecule; a molecule was selected at random and a random rotation around the center of mass was assigned. Rotational moves are not necessary for spherical particles.

The simulation box used (100.0 Å×100.0 Å×100.0 Å) contained one SWCNT. Simulations with larger boxes showed that finite-size effects did not exist when the above boxes were used. Similar to our previous work [45], an SWCNT was chosen as the adsorbent because it possesses straight cylindrical pores and has no preferred adsorption sites in the axial direction [50]. A cutoff radius of 17.0 Å was applied to the LJ interactions. Periodic boundary conditions were applied in all three dimensions. For each state point, CMC simulations consisted of 1×10^7 steps to guarantee equilibration, followed by 1×10^7 steps to sample the desired thermodynamic properties. In addition, to obtain a visual picture of the physical adsorption of He and Ne molecules on the SWCNT, we selected some snapshots of the configurations in the simulation boxes, as shown in Fig. 1.

The number of gas molecules in the simulation box (a box with dimensions of 100.0 Å×100.0 Å×100.0 Å) can be easily calculated at a particular temperature and pressure using the ideal gas equation of state. In the present work, the ideal gas assumption for the bulk phase was used.

Furthermore, to obtain adsorption isotherms, the gravimetric storage capacity (the absolute value of adsorption per mass of adsorbent), ρ_W, was calculated as follows:

$$\rho_W = \frac{N_{gas}.m_{gas}}{N_{gas}.m_{gas} + N_C.m_C}, \quad (4)$$

where N_{gas} and N_c are the number of gas molecules and carbon atoms in the simulation box, and m_{gas} and m_c (g mol^{-1}) are the corresponding molar masses, respectively.

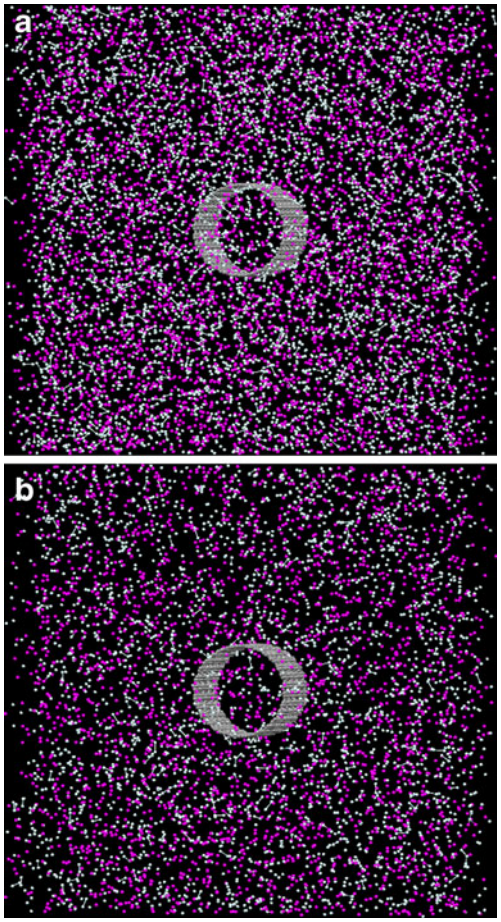

Fig. 1 **a**–**b** Snapshots of the CMC simulation box of the SWCNT at **a** 77 K and **b** 130 K and under 10 MPa pressure

Results and discussion

Adsorption isotherms

The gravimetric adsorption capacities of the He and Ne on the (15, 15) SWCNT [total, inner and outer, according to Eq. 4] were evaluated by feeding the LJ potential into the CMC simulation. The adsorption isotherms for He and Ne at subcritical (4 and 40 K) and supercritical (77 and 130 K) temperatures were obtained for a constant temperature and constant SWCNT diameter and length but varying pressure. The adsorption isotherms of He and Ne obtained at different temperatures are shown in Figs. 2, 3 and 4. All of the adsorption isotherms obtained for the He and Ne mixture were type I (Langmuir shape). An inherent property of type I isotherms is that adsorption is limited to the completion of a single monolayer of adsorbate at the adsorbent surface. Type I isotherms (parabolic behavior) are observed for the adsorption of gases onto microporous solids whose pore sizes are not much larger than the molecular diameter of the adsorbate; completely filling these narrow pores corresponds to the completion of a molecular monolayer [51]. Also, when the SWCNT radius is larger than approximately 2 nm, capillary condensation occurs when the temperature is sufficiently low, following the layer-by-layer adsorption of gas molecules onto the nanotube surface. When the SWCNT diameter is less than

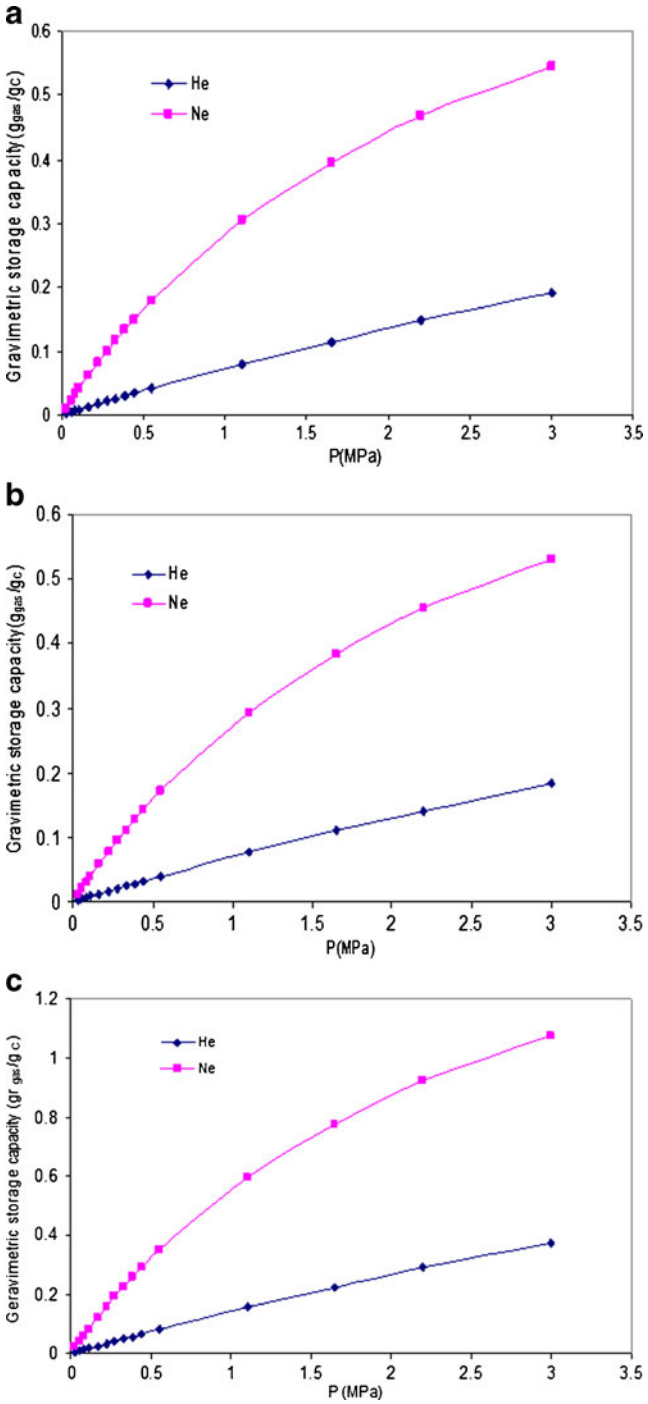

Fig. 2 **a**–**c** He and Ne adsorption isotherms measured at 4 K for **a** inner, **b** outer, and **c** total gravimetric storage capacities on the (15, 15) nanotube

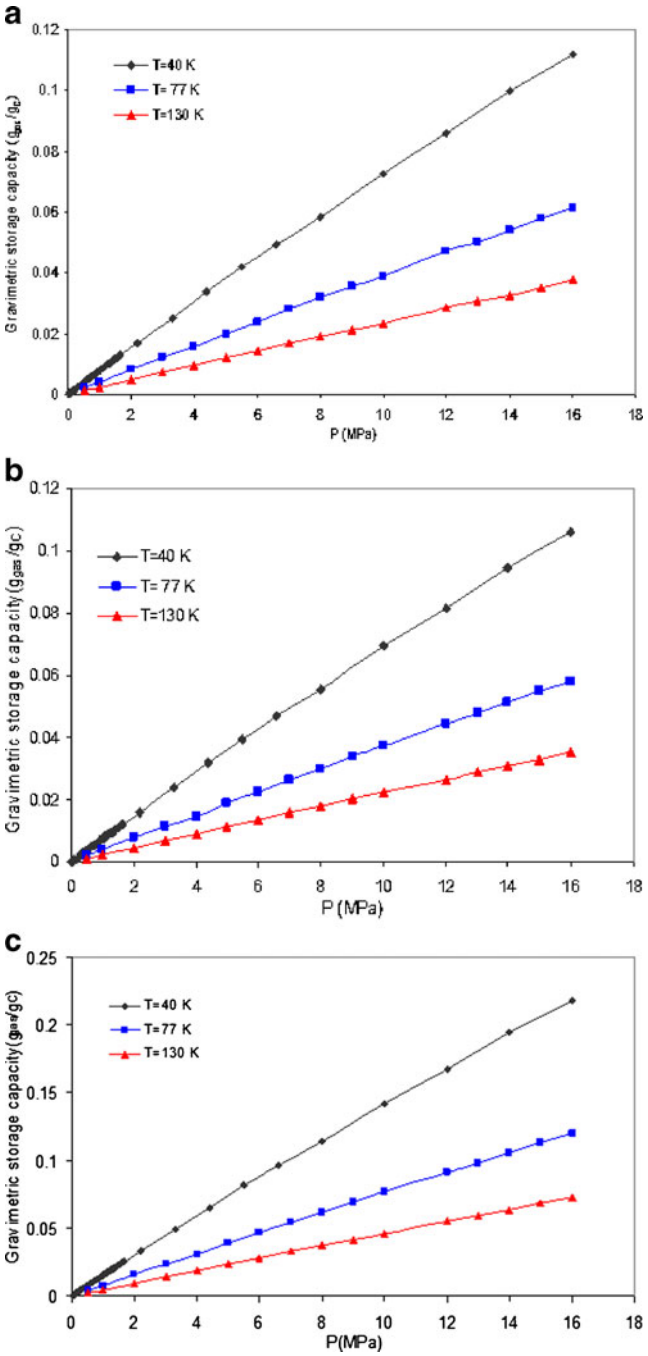

Fig. 3 **a**–**c** He adsorption isotherms measured at various temperatures for **a** inner, **b** outer, and **c** total gravimetric storage capacities on the (15, 15) nanotube

about 2 nm, no condensation is observed because the system becomes essentially one-dimensional [52]. Also, the contribution of gas–gas repulsion in the second layer is much larger than the predicted total energy contribution resulting from attractive forces (van der Waal's interaction of the gas with the surface of the tube). Thus, the gas adsorbed in the second layer would appear to be thermodynamically unstable. Adsorption isotherms are observed for the adsorption of He and Ne on (15, 15) nanotubes, implying that condensation is prohibited. Capillary condensation occurs when each pore is large enough to hold more than four layers of molecules. Our approach was validated by comparing them with the experimental results for Ne adsorption [40] and molecular simulation results for the Xe/Ar mixture [32].

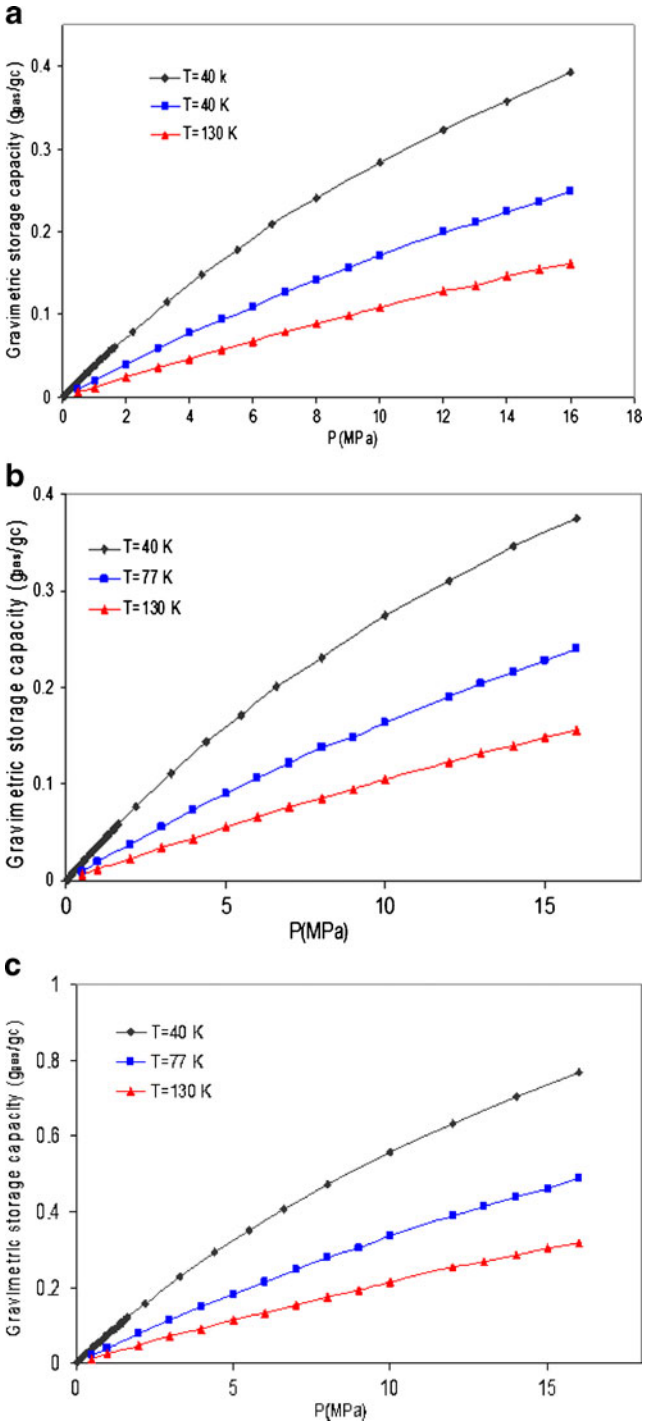

Fig. 4 **a**–**c** Ne adsorption isotherms measured at various temperatures for **a** inner, **b** outer, and **c** total gravimetric storage capacity on the (15, 15) nanotube

The adsorption isotherms for an equimolar He and Ne mixture are plotted in separate figure (Fig. 2) at 4 K as a function of pressure. It is clear that the magnitude of ρ_W for He gas fluctuates greatly from 0.55 wt% at 4 K to 0.125 wt% at 40, 77, and 130 K, and so parabolic behavior is not readily apparent for 40, 77 and 130 K. Thus, ρ_W was drawn in two separate diagrams.

Both the He and the Ne adsorption isotherms exhibit similar behavior, and the amount of He and Ne adsorbed on the inner surface of SWCNT is slightly more than that adsorbed on the outside. The accessible volume inside the tube is large because greater penetration is possible closer to the solid–fluid boundary due to the deeper solid–fluid potentials. It was shown that confinement in the inner volume of the nanotube is energetically more favorable than it is on the external surface. The optimum distances between the gas molecules (O_2, N_2 and NO) and the tube on its outer surface were found in previously published papers [43, 44] using DFT calculations, in order to show how the gas molecules were adsorbed onto the outer surface. Therefore, all of the gas molecules that were located in this region were considered to be adsorbed. If we compare the amounts of He and Ne adsorbed, Fig. 2 shows that more Ne is adsorbed than He for the pressure range specified. This is due to the fact that the gas molecules can vary considerably in size, physical properties (boiling point), structure, and electric properties (dipole and quadrupole moments). Hence, Ne adsorption is higher than He adsorption for the same conditions. The adsorption isotherms obtained for an equimolar mixture of He and Ne at different temperatures (40, 77, and 130 K) for the inner, outer, and total gravimetric storage capacities are shown in Figs. 3 and 4. These figures show that the ρ_W values of He and Ne increase with increasing gas pressure. Also, with increasing temperature, the amount of gas adsorbed increases. Similar to Fig. 2, Figs. 3 and 4 show that more Ne is adsorbed than He. According to Figs. 3 and 4, the (15, 15) SWCNT also shows preferential adsorption of Ne rather than the smaller noble gas He.

Figure 5a shows the phase diagram for a mixture of He and Ne at 4 K and 0.2 MPa. This figure plots x_{He} , the He composition of the adsorbed phase, as a function of y_{He} , the He composition in the bulk. The phase diagrams for two isobars, 1.0 MPa at 4 K and 0.2 MPa at 40 K, are also given in Figs. 6a and 7a. Figure 5b shows the adsorption isotherms for a He and Ne mixture at 4 K and 0.2 MPa as a function of y_{He}. The amount of He adsorbed increases monotonically with increasing y_{He}, and that for Ne decreases monotonically. In addition, similar to Fig. 5b, Figs. 6b and 7b show the adsorption isotherms for a He and Ne mixture at 4 K and 1.0 MPa and 40 k and 0.2 MPa as a function of y_{He}. There is a monotonic increase in the adsorbed He but a monotonic decrease in Ne with increasing y_{He} . Comparing the adsorption isotherms shown in Figs. 5b, 6b, and 7b, as it can be seen that the adsorption of He increases with increasing pressure at constant temperature (see Figs. 5b and 6b), while the adsorption of He decreases with increasing temperature at constant pressure (see Figs. 5b

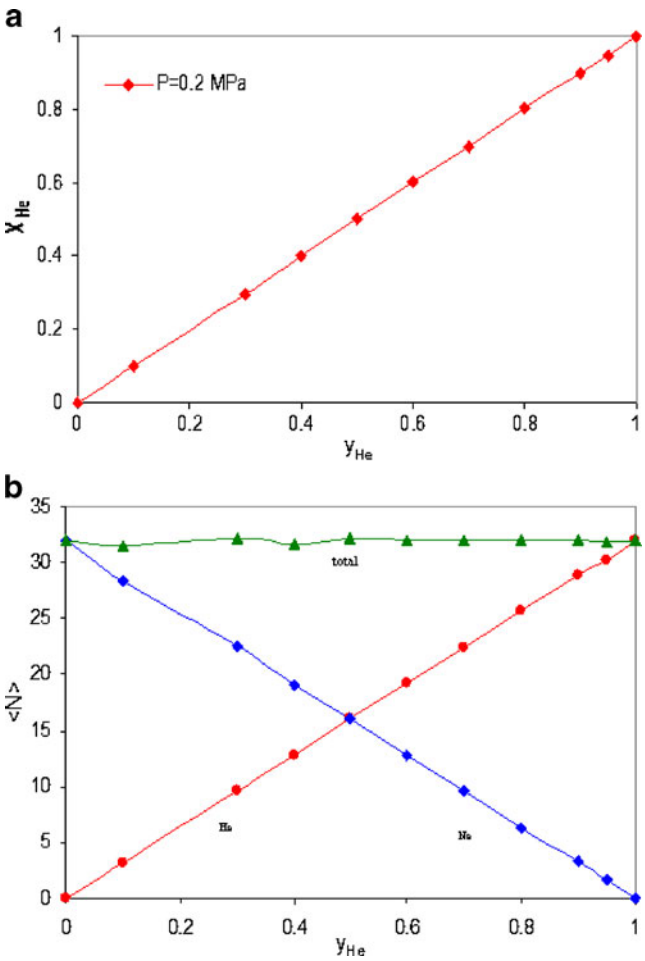

Fig. 5 **a**–**b** Adsorption of a He and Ne mixture inside nanotubes at 4 K and P=0.2 MPa as a function of the He bulk composition. **a** He composition in the adsorbed phase; **b** average number of adsorbed gas molecules

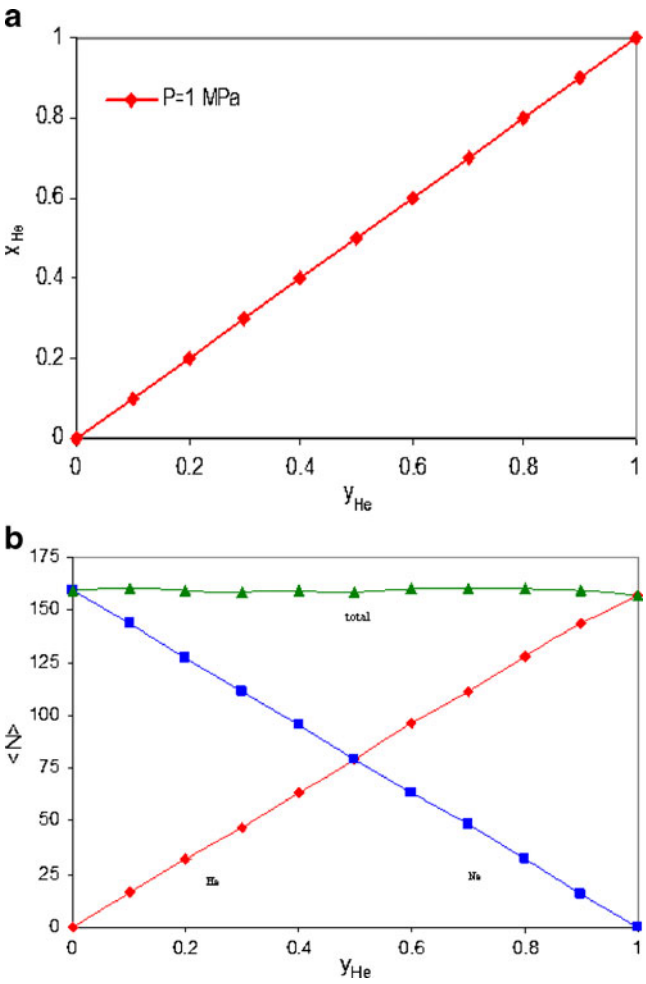

Fig. 6 **a**–**b** Adsorption of a He and Ne mixture inside nanotubes at 4 K and P=1 MPa as a function of the He bulk composition. **a** He composition in the adsorbed phase; **b** average number of adsorbed gas molecules

and 7b). As result, increasing pressure and increasing temperature have opposite effects on the adsorption of He.

Separation factors

To gain better insight into the separation, we analyzed the effects of pressure and temperature on the selectivity. In a mixture adsorption, the selectivity (or separation factor) of component i with respect to j is defined by S_{ij},

$$S_{ij} = \frac{x_i/y_i}{x_j/y_j}, \tag{5}$$

where x_i and y_i are the compositions of component i in the adsorbed and bulk phases, respectively.

Selectivity is a key parameter for quantifying the competitive adsorption between two components. When $S_{ij} > 1$, component i is preferentially adsorbed; in contrast, if $S_{ij} < 1$, component j is preferentially adsorbed. Of course, S_{ij}=1 implies that there is no competition; this is the isoselective point (ISP) at which there is a reversal in selectivity from $S_{ij} > 1$ to $S_{ij} < 1$ or vice versa.

Separation factors depend upon the nature of the adsorbate–adsorbent interactions; that is, on whether the surface is polar, nonpolar, hydrophilic, hydrophobic, etc., and on the process conditions used, such as temperature, pressure, and concentration. To achieve a practical separation based on kinetics, the size of the adsorbent micropores must be comparable with the dimensions of the diffusing adsorbate molecules.

Figure 8 shows the selectivity of Ne compared to He, $S_{Ne/He}$, as a function of the bulk composition of Ne. First we analyzed the effect of pressure on the separation factor at constant temperature. As shown in Fig. 8a, the separation factors at two different pressures (0.2 and 1.0 MPa) and a constant temperature (4 K) show different behaviors. At low pressure (0.2 MPa), the selectivity drops with increasing gas bulk composition until y_{Ne}=0.2 (20% of the gas

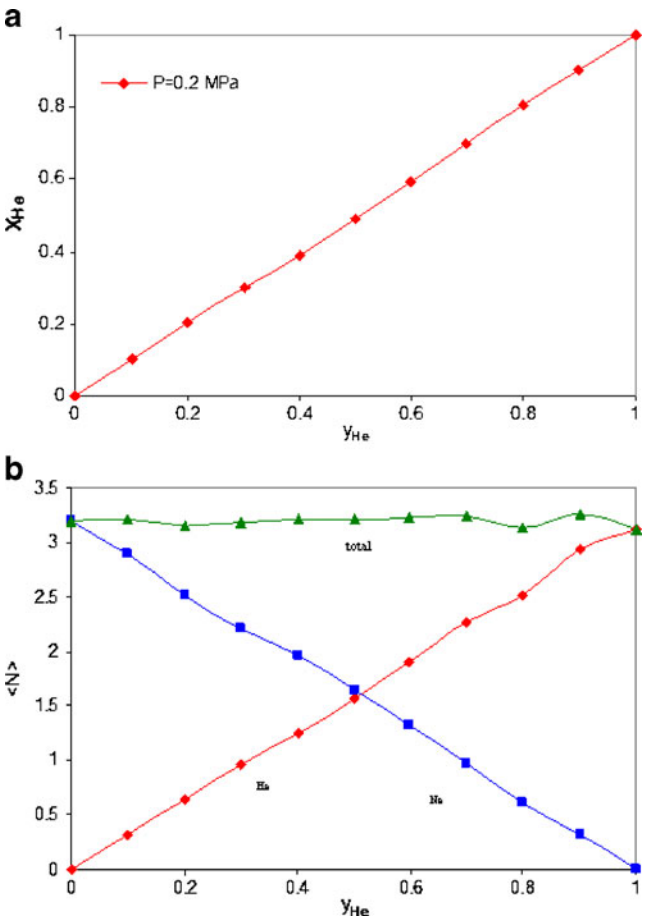

Fig. 7 **a**–**b** Adsorption of a He and Ne mixture inside nanotubes at 40 K and P=0.2 MPa as a function of the He bulk composition. **a** He composition in the adsorbed phase; **b** average number of adsorbed gas molecules

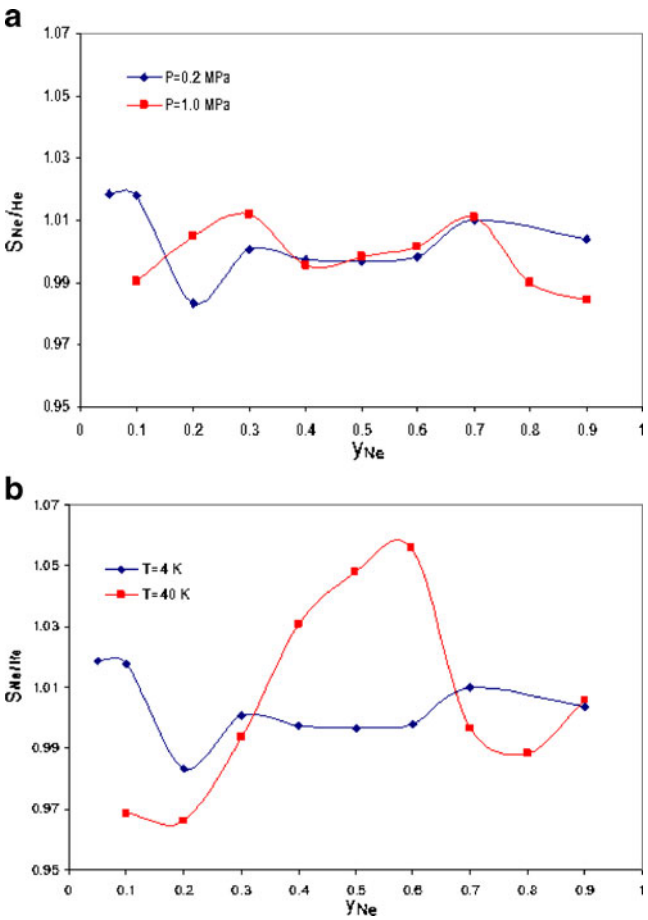

Fig. 8 **a**–**b** Selectivity of Ne compared to He as a function of the Ne bulk composition at **a** T=4 K, and **b** P=0.2 MPa

bulk is Ne and 80% is He). At a lower gas bulk of Ne, the selectivity is less than 1, and hence He is preferentially adsorbed. Furthermore, at a higher pressure (1.0 MPa), as the gas bulk composition increases, the selectivity reaches a maximum until y_{Ne}=0.3 (30% of the gas bulk is Ne and 70% is He). In other words, preferential adsorption of Ne occurs at this composition. According to Fig. 8a, the gas bulk composition shows isoselective point behavior for y_{Ne}=0.3 to 0.6. Comparing the results for the two pressures shows that the selectivities are largely dependent on the bulk gas composition. Preferential adsorption of Ne and He occurs at a gas bulk composition of less than y_{Ne}=0.3 and more than y_{Ne}=0.7. Our simulation results for the separation factor are in agreement with the molecular simulation results for the adsorption and separation of noble gases in metal–organic frameworks [32].

Second, the effect of temperature (4 and 40 K) on the selectivity of Ne compared to He (Fig. 8b) at a constant pressure (0.2 MPa) was investigated. As can be seen in Fig. 8b, at a higher temperature (40 K), the selectivity of Ne increases with increasing gas bulk composition until it reaches a maximum at y_{Ne}=0.55 (55% of the gas bulk is Ne and 45% is He). After this maximum, the selectivity decreases with increasing gas bulk composition. As the results show, at a higher temperature, the separation factors occur in the range of y_{Ne}=0.3 to y_{Ne}=0.65 of the bulk composition; at a lower temperature, separation does not occur in this range of gas bulk compositions. In other words, the preferential adsorption of Ne is dependent on the bulk gas composition (y_{Ne}=0.3 to y_{Ne}=0.65) at the higher temperature (40 K). In contrast, at the lower temperature (4 K), the selectivity is independent of the bulk gas composition. The selectivity of Ne is higher than that of He due to the adsorbate–adsorbate interactions. In other words, Ne–Ne interactions are stronger than He–He interactions, which means that the ratio $\varepsilon_{Ne}/\varepsilon_{He}$ is larger than the ratio $\varepsilon_{He}/\varepsilon_{Ne}$.

Isosteric enthalpy

Calculating the isosteric enthalpies of adsorption for a specific surface coverage requires accurate interpolation

between isotherm points to obtain the pressures for specific surface coverages for isotherms obtained at various temperatures, and this requires the use of isotherm models. The most appropriate model to use depends on the shape of the isotherm. Limited heat data is generally available for pure gas adsorption, heat data for binary gas mixtures are rare, and heat data for mixtures containing three or more components are nonexistent.

In this research work, we obtained isosteric enthalpies of adsorption (coverage-dependent isosteric heats of adsorption) by fitting the adsorption data. To extract the isosteric enthalpies of adsorption, the data were modeled with a virial-type expression consisting of the parameters a_i and b_i that are independent of temperature [53]:

$$\ln P = \ln N + \frac{1}{T}\sum_{i=0}^{m} a_i N^i + \sum_{i=0}^{n} b_i N^i, \quad (6)$$

where P is the pressure, N is the amount adsorbed, T is the temperature, and m and n determine the number of terms required to adequately describe the isotherm. Aspects of this equation and its use to study CH_4, CF_4, SF_6, and H_2 adsorbed on activated carbon [54, 55] and H_2 [19], and D_2 [56] adsorbed on a metal–organic framework (MOF) have been previously described. To fit the data, the Mathematica 8 software package was used, and the successive terms used in all cases were $m \leq 5$ and $n \leq 3$. The isosteric enthalpy of adsorption (Q_{st}) was obtained using the following equation:

$$Q_{st} = -R\sum_{i=0}^{m} a_i N^i, \quad (7)$$

where R is the gas constant. The quantity Q_{st} is the heat of compression arising from the transformation of a gas of finite volume into an adsorbed layer of essentially zero volume.

The isosteric enthalpy of adsorption (Q_{st}) for a gas adsorbed on the inner surface of the tube was calculated by fitting the 4, 40, 77, and 130 K isotherm adsorption data presented graphically in Fig. 9.

Figure 9 shows the isosteric enthalpies of adsorption of He and Ne as a function of the amount of gas adsorbed. Similar to the adsorption isotherms and separation factors, Q_{st} for Ne is larger than that for He under identical conditions. The isosteric enthalpies of adsorption for He and Ne show gradual, near-linear decreases in their values as a function of the amount of gas adsorbed. Such behavior has been observed experimentally, for example in the adsorption of H_2 on an MOF [19]. The decrease in Q_{st} results from additional admolecules having to occupy an energetically less favorable adsorption region, leading to a weaker adsorbate–adsorbent attraction, and a weaker adsorbate-adsorbate attraction due to the shorter distance between the admolecules in the limited space available [29].

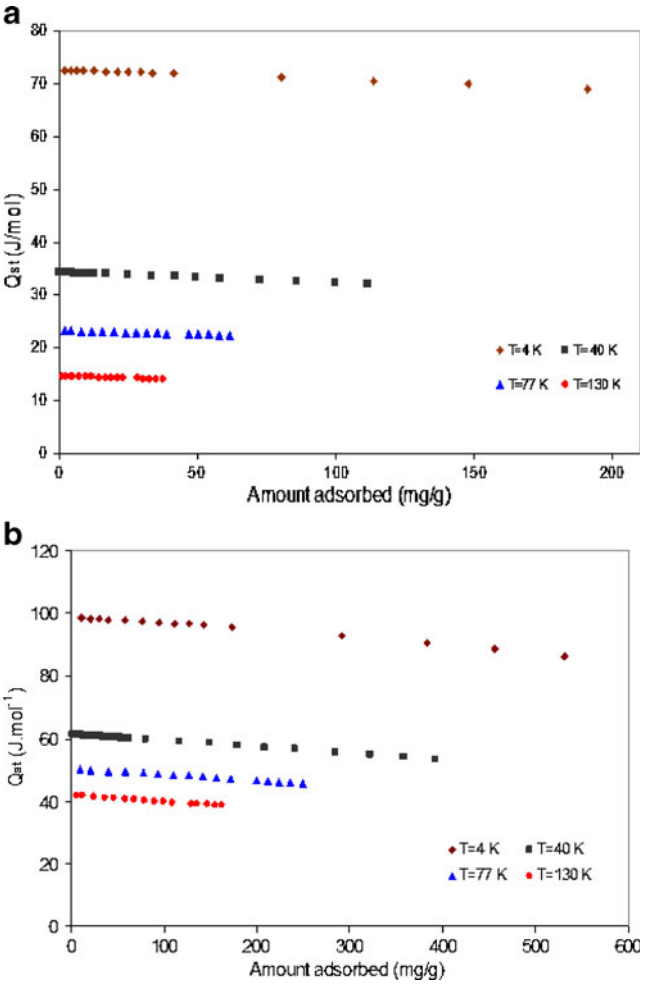

Fig. 9 **a**–**b** Variation of the isosteric enthalpy of adsorption (Q_{st}/J mol^{-1}) with the amount of gas adsorbed (mg g^{-1}) inside nanotubes at different temperatures. **a** He; **b** Ne

The behavior of Q_{st} with temperature is quite interesting. A modest maximum Q_{st} was observed at the lower temperature (4 K) and a minimum Q_{st} at the higher temperature (130 K) for both He and Ne. The results obtained for Q_{st} are in agreement with a theoretical study of Ar adsorption onto carbon nanotubes [56] at <200 K. The distribution of adsorbate is governed by the Boltzmann factor, $\exp(-E/kT)$. At a low temperature, the higher energy adsorption sites are preferentially filled (more thermodynamic work done by the adsorption process [57]). The lower energy sites are preferentially filled at a high temperature. In addition, as the amount of adsorbate increases, the distance between the adsorbates decreases. Lateral interactions become increasingly likely, and these can influence Q_{st}, leading to changes as a function of the amount of adsorbate. Comparative studies reveal that, under identical conditions,

the isosteric enthalpy of adsorption of Ne obtained from fitting is higher than that of He (see Fig. 9a and b). This means that the adsorbate–adsorbate interactions are more important for Ne. The data obtained from the adsorption isotherms are in good agreement with the results obtained for the isosteric enthalpies of adsorption.

Conclusions

In this paper, we showed that CMC simulation is a useful tool for studying the microscopic adsorptive behavior of helium and neon mixtures on carbon nanotubes. We considered the adsorption of helium and neon on both the inner and outer surfaces of the tubes at different temperatures (4, 40, 77, and 130 K) for the pressure range of 1–16 MPa. All of the adsorption isotherms obtained were of type I at both subcritical and supercritical temperatures. The adsorption isotherms also show that more gas is always adsorbed on the inner surfaces of the tubes rather than the outer surfaces. Comparisons of the adsorption isotherms of He and Ne mixtures indicate that there are significant differences between the isotherms. In the pressure range studied, more Ne was adsorbed than He. Competitive adsorption occurs in gas mixtures because of size differences between the components. The results for the separation factors show that the selectivities are largely dependent on the bulk gas composition. As the results show, there is a preference for Ne adsorption rather than He adsorption from a Ne/He mixture at most bulk compositions because the adsorbate–adsorbate interactions of Ne are stronger than those of He. In addition, the isosteric enthalpies of adsorption for He and Ne showed gradual, near-linear decreases in their values as a function of the amount of gas adsorbed. Similar to the adsorption isotherms and separation factors, Q_{st} of Ne is larger than that of He under identical conditions.

References

1. Migone AD, Talapatra S (2004) Encyclopedia of nanoscience and nanotechnology. American Scientific Publishers, Los Angeles
2. Calbi MM, Gatica SM, Bojan MJ, Cole MW (2001) Phases of neon, xenon, and methane adsorbed on nanotube bundles. J Chem Phys 115:9975–9981
3. Politzer P, Lane P, Murray JS, Concha MC (2005) Comparative analysis of surface electrostatic potentials of carbon, boron/nitrogen and carbon/boron/nitrogen model nanotubes. J Mol Model 11:1–7
4. Calbi MM, Cole MW (2002) Dimensional crossover and quantum effects of gases adsorbed on nanotube bundles. Phys Rev B 66:115413–115412
5. Talapatra S, Zhambano AJ, Weber SE, Migone AD (2000) Gases do not adsorb on the interstitial channels of close-ended single-walled carbon nanotube bundles. Phys Rev Lett 85:138–141
6. Talapatra S, Migone AD (2001) Existence of novel quasi-one-dimensional phases of atoms adsorbed on the exterior surface of close-ended single wall nanotube bundles. Phys Rev Lett 87:206106–206109
7. Talapatra S, Rawat DS, Migone AD (2002) Possible existence of a higher coverage quasi-one-dimensional phase of argon adsorbed on bundles of single-walled carbon nanotubes. J Nanosci Nanotechnol 2:467–470
8. Rawat DS, Heroux L, Krungleviciute V, Migone AD (2006) Adsorption of xenon on purified HiPco single walled carbon nanotubes. Langmuir 22:234–238
9. Bienfait M, Zeppenfeld P, Dupont-Pavlovsky N, Muris M, Johnson MR, Wilson T, DePies M, Vilches OE (2004) Thermodynamics and structure of hydrogen, methane, argon, oxygen, and carbon dioxide adsorbed on single-wall carbon nanotube bundles. Phys Rev B 70:035410–035419
10. Muris M, Dupont-Pavlovsky N, Bienfait M, Zeppenfeld P (2001) Where are the molecules adsorbed on single-walled nanotubes? Surf Sci 492:67–74
11. Rawat DS, Furuhashi T, Migone AD (2009) Study of a butane monolayer adsorbed on single-walled carbon nanotubes. Langmuir 25:973–976
12. Mao Z, Sinnott SB (2002) Predictions of a spiral diffusion path for nonspherical organic molecules in carbon nanotubes. Phys Rev Lett 89:278301–278304
13. Jiang J, Sandler SI, Schenk M, Smit B (2005) Adsorption and separation of linear and branched alkanes on carbon nanotube bundles from configurational-bias Monte Carlo simulation. Phys Rev B 72:045447–045456
14. Kondratyuk P, Wang Y, Johnson JK, Yates JTJ (2005) Observation of a one-dimensional adsorption site on carbon nanotubes: adsorption of alkanes of different molecular lengths. J Phys Chem B 109:20999–21005
15. Funk S, Burghaus U, White B, O'Brien S, Turro NJ (2007) Adsorption dynamics of alkanes on single-wall carbon nanotubes: a molecular beam scattering study. J Phys Chem C 111:8043–8049
16. Rawat DS, Migone AD (2007) Phases of ethane adsorbed on purified HiPco single-walled carbon nanotubes. Phys Rev B 75:195440–195444
17. Iijima S (1991) Helical microtubules of graphitic carbon. Nature 354:56–58
18. Lithoxoos GP, Samios J, Carissan Y (2008) Investigation of silicon model nanotubes as potential candidate nanomaterials for efficient hydrogen storage: a combined ab initio/grand canonical Monte Carlo simulation study. J Phys Chem C 112:16725–16728
19. Rowsell JLC, Yaghi OM (2006) Effects of functionalization, catenation, and variation of the metal oxide and organic linking units on the low-pressure hydrogen adsorption properties of metal–organic frameworks. J Am Chem Soc 128:1304–1315
20. Yoo DH, Rue GH, Chan MHW, Hwang YH, Kim HK (2003) Study of nitrogen adsorbed on open-ended nanotube bundles. J Phys Chem B 107:1540–1542
21. Collins DJ, Zhou HC (2007) Hydrogen storage in metal-organic frameworks. J Mater Chem 17:3154–3160
22. Muris M, Dufau N, Bienfait M, Dupont-Pavlovsky N, Grillet Y, Palmari JP (2000) Methane and krypton adsorption on single-walled carbon nanotubes. Langmuir 16:7019–7022
23. Zhao XB, Xiao B, Fletcher AJ, Thomas KM (2005) Hydrogen adsorption on functionalized nanoporous activated carbons. J Phys Chem B 109:8880–8888
24. Ribeiro RP, Sauer TP, Lopes FV, Moreira RF, Grande CA, Rodrigues AE (2008) Adsorption of CO_2, CH_4, and N_2 in activated carbon honeycomb monolith. J Chem Eng Data 53:2311–2317

25. Ruangpornvisuti V (2009) Molecular modeling of dissociative and non-dissociative chemisorption of nitrosamine on close-ended and open-ended pristine and Stone–Wales defective (5, 5) armchair single-walled carbon nanotubes. J Mol Model 16:1127–1138
26. Wang Q, Johnson JK (1999) Optimization of carbon nanotube arrays for hydrogen adsorption. J Phys Chem B 103:4809–4813
27. Knippenberg TM, Stuart SJ, Cheng H (2008) Molecular dynamics simulations on hydrogen adsorption in finite single walled carbon nanotube bundles. J Mol Model 14:343–351
28. Mykhailenko O, Matsui D, Prylutskyy Y, Le Normand F, Eklund P, Scharff P (2007) Monte Carlo simulation of intercalated carbon nanotubes. J Mol Model 13:283–287
29. Jiang J, Sandler SI (2005) Separation of CO_2 and N_2 by adsorption in C168 schwarzite: a combination of quantum mechanics and molecular simulation study. J Am Chem Soc 127:11989–11997
30. Qiao S, Wang K, Hu X (2000) Study of binary adsorption equilibrium of hydrocarbons in activated carbon using micropore size distribution. Langmuir 16:5130–5136
31. Jiang J, Wagner NJ, Sandler SI (2004) A Monte Carlo simulation study of the effect of carbon topology on nitrogen adsorption on graphite, a nanotube bundle, C_{60} fullerite, C168 schwarzite, and a nanoporous carbon. Phys Chem Chem Phys 6:4440–4444
32. Greathouse JA, Kinnibrugh TL, Allendorf MD (2009) Adsorption and separation of noble gases by IRMOF-1: grand canonical Monte Carlo simulations. Ind Eng Chem Res 48:3425–3431
33. Mueller U, Schubert M, Teich F, Puetter H, Schierle-Arndt K, Pastre J (2006) Metal–organic frameworks—prospective industrial applications. J Mater Chem 16:626–636
34. Grigoriev IM, Tonkov MV, Frommhold L (1998) Interaction-induced dipole and absorption spectra of collisional Ar–Xe pairs. Phys Rev A 58:4978–4980
35. Meuwly M, Doll JD (2002) Dynamical studies of mixed rare-gas clusters: collision-induced absorption in $(Ne)_n$–$(Ar)_m$ (n+m <= 100). Phys Rev A 66:023202–023210
36. Dawid A, Gburski Z (1998) Interaction-induced absorption in argon–krypton mixture clusters: molecular-dynamics study. Phys Rev A 58:740–743
37. Do DD, Do HD, Wongkoblap A, Nicholson D (2008) Henry constant and isosteric heat at zero-loading for gas adsorption in carbon nanotubes. Phys Chem Chem Phys 10:7293–7303
38. Jalili S, Vaez A (2007) Xenon adsorption on defected single-walled carbon nanotubes. Chem Phys Lett 437:233–237
39. Firlej L, Kuchta B (2004) Helium adsorption in single wall carbon nanotubes—grand canonical Monte Carlo study. Colloid Surf A 241:149–154
40. Krungleviciute V, Heroux L, Talapatra S, Migone AD (2004) Gas adsorption on HiPco nanotubes: surface area determinations, and neon second layer data. Nano Lett 4:1133–1137
41. Do DD, Do H (2005) Cooperative and competitive adsorption of ethylene, ethane, nitrogen and argon on graphitized carbon black and in slit pores. Adsorption 11:35–50
42. Schindler BJ, LeVan MD (2008) The theoretical maximum isosteric heat of adsorption in the Henry's law region for slit-shaped carbon nanopores. Carbon 46:644–648
43. Rafati AA, Hashemianzadeh SM, Nojini ZB (2008) Electronic properties of adsorption nitrogen monoxide on inside and outside of the armchair single wall carbon nanotubes: a density functional theory calculations. J Phys Chem C 112:3597–3604
44. Rafati AA, Hashemianzadeh SM, Nojini ZB (2009) Effect of the adsorption of oxygen on electronic structures and geometrical parameters of armchair single-wall carbon nanotubes: a density functional study. J Colloid Interface Sci 336:1–12
45. Rafati AA, Hashemianzadeh SM, Nojini ZB, Naghshineh N (2010) Canonical Monte Carlo simulation of adsorption of O_2 and N_2 mixture on single walled carbon nanotube at different temperatures and pressures. J Comput Chem 31:1443–1449
46. Steele WA (1973) Physical interaction of gases with crystalline solids. I. Gas–solid energies and properties of isolated adsorbed atoms. Surf Sci 36:317–352
47. Morales JJ, Nuevo MJ (1995) Path-integral molecular-dynamics methods—application to neon. J Comput Chem 16:105–112
48. Allen MP, Tildesley DJ (1987) Computer simulation of liquids. Clarendon, Oxford
49. Frenkel D, Smit B (2002) Understanding molecular simulation: from algorithms to applications. Elsevier, New York
50. Zhao JJ, Buldum A, Han J, Lu JP (2002) Gas molecule adsorption in carbon nanotubes and nanotube bundles. Nanotechnology 13:195–200
51. Thomas WJ, Crittenden B (1998) Adsorption technology and design. Elsevier, Amsterdam
52. Cao D, Wu JZ (2004) Self-diffusion of methane in single-walled carbon nanotubes at sub- and supercritical conditions. Langmuir 20:3759–3765
53. Czepirski L, Jagiello J (1989) Virial-type thermal equation of gas–solid adsorption. J Chem Eng Sci 44:797–801
54. Jagiello J, Bandosz TJ, Putyera K, Schwarz JA (1995) Adsorption near ambient temperatures of methane, carbon tetrafluoride, and sulfur hexafluoride on commercial activated carbons. J Chem Eng Data 40:1288–1292
55. Anson A, Jagiello J, Para JB, Sanjuan ML, Benito AM, Maser WK, Martinez MT (2004) Porosity, surface area, surface energy, and hydrogen adsorption in nanostructured carbons. J Phys Chem B 108:15820–15826
56. Chen B, Zhao X, Putkham A, Hong K, Lobkovsky EB, Hurtado EJ, Fletcher AJ, Thomas KM (2008) Surface interactions and quantum kinetic molecular sieving for H_2 and D_2 adsorption on a mixed metal–organic framework material. J Am Chem Soc 130:6411–6423
57. Sircar S, Cao DV (2002) Heat of adsorption. Chem Eng Technol 25:945–948